MECSOL 2022 - Proceedings of the 8th International Symposium on Solid Mechanics
M.L. Bittencourt, J. Labaki, L.C.M. Vieira Jr. and E. Mesquita (Editors), Campinas SP, Brazil, October 17th to 19th, 2022

Flexible Rail Representation on Multibody Dynamics Using a Quadratic Finite Element Based on the Absolute Nodal Coordinate Formulation

Leonardo Bartalini Baruffaldi[1], Auteliano Antunes dos Santos Jr.[1] and Marco Lúcio Bittencourt[2]

[1] Instituto Federal de São Paulo, câmpus Hortolândia. Avenida Thereza Ana Cecon Breda, 1896 - Vila São Pedro - Hortolândia, SP (Brazil). E-mail: leonardo.baruffaldi@ifsp.edu.br
[2] University of Campinas, Mechanical Engineering Faculty. Rua Mendeleev, 200 - Cidade Universitária - Campinas, SP (Brazil)

Abstract. The design and analysis of railway vehicles has, for many years now, relied on multibody system dynamics (MBD) modelling both to speed up the design cycle and reduce prototyping and instrumentation costs. The use of flexible rails within these models, however, is a problem that is not completely solved yet: early approaches used concentrated parameters to represent rail, sleepers, ballast, and other underrail elements; current state of the art commercial software rely on modal reduction extracted from finite element models; and recent advances walk towards finite elements integrated to the MBD solver or towards co-simulation between MBD and FEA. Based on the already established absolute nodal coordinate approach with the continuum mechanics formulation and selective integration, this work presents a quadratic, three-dimensional beam element that can be used to effectively model rails. The elements are implemented on a MBD code and integrated using kinematic constraints and the augmented lagrangian technique, yielding a differential algebraic equations system. A methodology for inverse mapping contact points between wheel and rail is also presented and results are shown, comparing element performance under different choices of integration points.
Keywords: multibody dynamics, finite element method, rail vehicle dynamics, track flexibility

INTRODUCTION

Like most contemporary transportation equipment, railroad vehicles design, development, and analysis rely heavily on computer simulations to decrease time to market, costs, avoid accidents, improve maintenance and increase reliability, among other motivations (Evans and Berg, 2009). Among the techniques used to achieve such goals, dynamical modeling by multibody systems is crucial, in that it provides information on accelerations, velocities, positions, forces and contact parameters that have direct impact on vehicle performance.

Let one assumes a system composed of n rigid bodies, each one associated to a moving reference frame attached to its center of gravity, with six degrees of freedom and connected via a set of m kinematic constraints and l forces. Then the general multibody problem can be reduced to the following set of index-1 differential-algebraic equations (DAE) of motion (Pfeiffer, 2005; Shabana, 2005):

$$\begin{bmatrix} \mathbf{M} & -\mathbf{G}^T \\ \mathbf{G} & \mathbf{0} \end{bmatrix} \begin{bmatrix} \ddot{\mathbf{z}} \\ \lambda \end{bmatrix} = \begin{bmatrix} -\mathbf{h} \\ \mathbf{0} \end{bmatrix} + \begin{bmatrix} \mathbf{f} \\ \mathbf{0} \end{bmatrix} \tag{1}$$

where

$\mathbf{M}$	is the inertia matrix
$\mathbf{G} = G_{ij} = \frac{dg_i}{dz_j}$	is the jacobian of the constraint equations
$\ddot{\mathbf{z}}$	is the vector with the second time derivative of the position coordinates
λ	is the vector of Lagrange multipliers associated to the constraints
$\mathbf{h}$	is the vector containing nonlinear terms related to angular speeds
$\mathbf{f}$	is the vector with active efforts applied to the system.

Equations (1) can be manipulated to yield either index-2 or index-3 DAE (a complete discussion on DAE indexes can be found in Ascher and Petzold (1998)), but independently of the final form, it is clear that constant $\mathbf{M}$ and $\mathbf{G}$ matrices are beneficial to the numerical solution because a single inversion decomposition can be made at the beginning of the solution procedure.

Railroad vehicles, however, are not entirely composed of bodies that can be regarded as rigid. Taking, for instance, the conventional three-piece-truck (Fig. 1) used in Brazilian and American freight transportation, Lima et al. (2022) showed

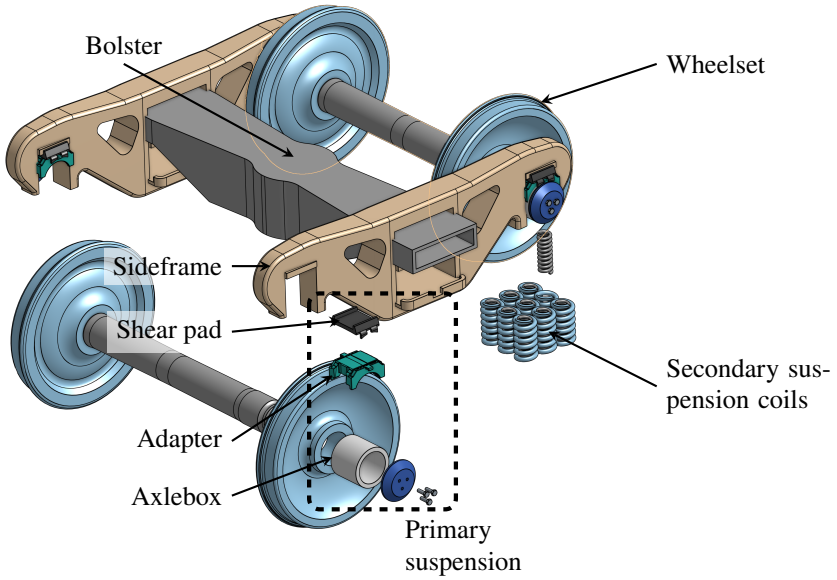

Figure 1 – Three-piece-truck used in heavy haul transportation.

that the vertical stiffness of the sideframe is comparable to that of the primary suspension. Not only parts of the vehicle are quite complaining, but also the track itself is known to be rather flexible in such a way that it can affect dynamic behavior. The problem of a beam laid down on an elastic foundation has been studied since the late XVIII century (Winkler, 1867), with major contributions by S. Timoshenko and collaborators occurring between 1920 and 1930 (Timoshenko, 1926). The subject of flexible track remained of little interest between late 1930's and early 1970's, when increases in train speeds showed that high frequency track response characteristics must be accounted for when analyzing railway vehicle dynamics. Knothe and Grassie (1993) provided a very comprehensive review of track modeling techniques (mainly focused on vertical responses) up to the beginning of the 1990 decade. Guimarães (1999) implemented a Timoshenko beam finite element model to analyze the vertical behavior of a track under a moving wheel with pots. Since then, several other authors have advanced on the subject. Shabana et al. (2008) and Shabana and Sanborn (2009) used the floating frame of reference formulation (FFRF) to develop a methodology to include a finite element description of the rails into a multibody model. On one hand, this approach, however, had the downside of resulting in a very nonlinear, time dependent mass matrix which, as discussed before, increase the computational cost of solving the differential-algebraic equations of motion. On the other hand, as developed later by Recuero et al. (2011), the floating frame of reference applied to modeling rail flexibility is prone to modal reduction via component mode synthesis, which selectively removes some degrees of freedom from the model. In the same paper, Recuero et al. (2011) extended the original elements from Shabana's group works cited earlier on this paragraph to include also under-rail pads, sleepers and ballast interaction. Antunes et al. (2019) developed a co-simulation technique to transfer data from a finite element specialized code into and from the mutibody solver, which implies in using two separate codes and to establish a communication protocol between them.

As its name suggests, the floating frame of reference formulation uses an intermediate coordinate system in which the deformations of the body are described. As such, the position of any point $\mathbf{r}_P$ of the body during the simulation is obtained by summing the position of the floating frame $\mathbf{r}_{FF}$ associated to the body with the displacements caused by deformation, which are described in local, i.e., in the floating frame system:

$$\mathbf{r}_P = \mathbf{r}_{FF} + \mathbf{A}_{FF} \cdot \left({}^{FF}\mathbf{u}_{0P} + {}^{FF}\mathbf{u}_P \right) \tag{2}$$

The second right-side term of (2) is composed of the sum of the time-independent undeformed position of point P in the floating frame of reference, ${}^{FF}\mathbf{u}_{0P}$, with the displacements caused by the deformation, ${}^{FF}\mathbf{u}_P$, which can be obtained by a finite element interpolation scheme applied to the nodal coordinates (please refer to the papers cited above to more details). These components are multiplied by $\mathbf{A}_{FF}$, which is the rotation matrix that converts from the floating frame to

the inertial frame. The ^{FF} superscript before the vectors indicate that they are written on a frame that is not the inertial one. This notation shall be kept from this point on in this paper.

Our goal is to propose a rail model that can be seamlessly integrated into equations (1) yielding a constant mass matrix. This can be achieved by using an absolute nodal coordinate formulation (ANCF) to describe the elements, instead of the FFRF cited before. The ANCF applied to beams was initially proposed by Prof. Shabana's research group at the University of Illinois Chicago (Shabana et al., 1997; Escalona et al., 1998; Shabana and Christensen, 1997) using cubic functions to interpolate both longitudinal and transverse displacements. These first movements towards the development of the technique showed that the internal force vectors, resulting from the strain field integration, were quite cumbersome to calculate. To mitigate the difficulty in obtained such force terms, Berzeri and Shabana (2000); Berzeri et al. (2001) developed a method to simplify them. Later on, a three-dimensional generalization of such elements was presented by Shabana and Yakoub (2001b,a), but now using a cubic polynomial to interpolate the longitudinal coordinate and linear functions to interpolate transverse coordinates. In order to solve the problem of shear locking that was noticed with the original ANCF elements, Nachbagauer et al. (2011, 2013b) proposed a selective reduced integration scheme applied to a quadratic element with rectangular cross section.

In this paper we present an element based on Nachbagauer et al. quadratic, selective reduced integration model, with adaptations to a rail cross-section.

THE ANCF FINITE ELEMENT FORMULATION

Contrary to the FFRF, absolute nodal coordinates elements rely on node coordinates that are written on the inertial frame of reference. Following the developments by Nachbagauer et al. (2011, 2013a), in this paper a quadratic beam element using the ANCF and a solid mechanics approach with reduced selective integration to cope with Poisson locking effects. A set of three natural coordinates $\boldsymbol{\xi} = [\xi, \eta, \zeta]$, all contained in a $[-1, 1]$ interval, are used to describe element length, height and width respectively.

The proposed element has three nodes located at the cross-section origin ($\eta = 0$ and $\zeta = 0$) with nine degrees of freedom each. These degrees of freedom are collected on a vector $\mathbf{q}^{(n)}$, where (n) informs the node number:

$$\mathbf{q}^{(n)} = \begin{bmatrix} \mathbf{q}_r^{(n)T} & \mathbf{q}_\eta^{(n)T} & \mathbf{q}_\zeta^{(n)T} \end{bmatrix}^T \tag{3}$$

In the equation above, $\mathbf{q}_r^{(n)}$ is the vector that informs the position of the node with respect to the inertial frame, $\mathbf{q}_\eta^{(n)}$ is the direction of the η axis of the cross-section, while $\mathbf{q}_\zeta^{(n)}$ is analogous to $\mathbf{q}_\eta^{(n)}$ considering natural coordinate ζ. Considering an initial configuration without any pre-deformation, both $\mathbf{q}_\eta^{(n)}$ and $\mathbf{q}_\zeta^{(n)}$ are defined as unitary and perpendicular. By taking their cross product it is possible, then, to define a local cartesian frame which can be used to transform quantities, like strains, from the material local frame into the inertial frame. Figure 2 shows a representation of nodal coordinates.

The nodal degrees of freedom vector $\mathbf{q}^{(n)}$ can be understood as composed by two separate parts: one that is related to its initial configuration $\mathbf{q}_0^{(n)}$ and the other one associated with its displaced configuration $\mathbf{u}^{(n)} = \begin{bmatrix} \mathbf{u}_r^{(n)T} & \mathbf{u}_\eta^{(n)T} & \mathbf{u}_\zeta^{(n)T} \end{bmatrix}^T$.

$$\mathbf{q}^{(n)} = \mathbf{q}_0^{(n)} + \mathbf{u}^{(n)} \tag{4}$$

Finally, the element degrees of freedom vector with 27 elements can be assembled as:

$$\mathbf{q}^{(e)} = \begin{bmatrix} \mathbf{q}^{(e1)T} & \mathbf{q}^{(e2)T} & \mathbf{q}^{(e3)T} \end{bmatrix}^T \tag{5}$$

where the superscripts $(e1)$, $(e2)$, and $(e3)$ indicate nodes number 1, 2, and 3 of the referred element.

Using a straightforward finite element interpolation scheme, the absolute coordinates of any point $\mathbf{r}_{P\in e}$ on the element can be calculated using a shape function matrix $\mathbf{S}$ such that

$$\mathbf{r}_{P\in e} = \mathbf{S}(\xi^\star, \eta^\star, \zeta^\star) \cdot \mathbf{q}^{(e)} = \mathbf{S}(\xi^\star, \eta^\star, \zeta^\star) \cdot \left(\mathbf{q}_0^{(e)} + \mathbf{u}^{(e)} \right) \tag{6}$$

The reader should notice that in Eq. 6 a starred version of the natural coordinates are used. This is because each natural coordinate varies from -1 to 1, while the element has arbitary length, width and height. Furthermore, supposing that an non-rectangular cross-section is used, one can establish the following relations between natural and starred coordinates:

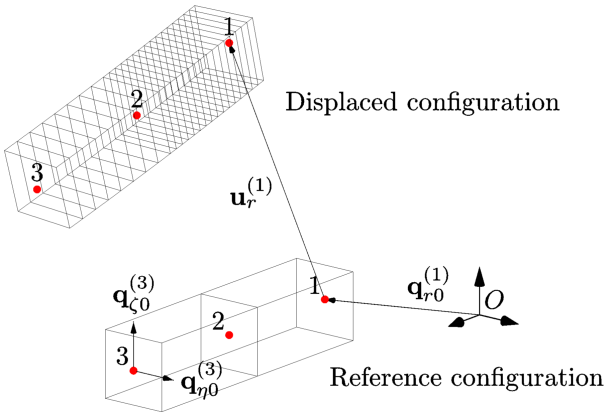

Figure 2 – Quadratic ANCF finite element definition. Vectors $\mathbf{q}_{r0}^{(1)}$ and $\mathbf{u}^{(1)}$ indicate the initial position and the displacement of node number 1 of the element. Vectors $\mathbf{q}_{\eta 0}^{(3)}$ and $\mathbf{q}_{\zeta 0}^{(3)}$ are the initial cross-section orientation vectors of node number 3. Point O references the origin of the inertial coordinate frame.

$$\xi^\star = \xi \cdot \frac{L}{2} \tag{7}$$

$$\eta^\star = \eta \cdot \frac{H}{2} \tag{8}$$

$$\zeta^\star = \zeta \cdot \frac{W(\eta^\star)}{2} \tag{9}$$

where L is element undeformed length, H is the element cross-section undeformed height, and W is the element cross-section undeformed width. Eq. 9 shows that $\zeta^\star$ depends on $\eta^\star$. Compared the formulation by Nachbagauer et al., that modification allows one to consider the non-rectangular cross-section of rails.

Because the shape function $\mathbf{S}$ in equation (6) is time-invariant, the absolute velocity of a point of the element is:

$$\dot{\mathbf{r}}_{P\in e} = \mathbf{S}(\xi^\star, \eta^\star, \zeta^\star) \cdot \dot{\mathbf{q}}^{(e)} \tag{10}$$

This result can be used to calculate the total kinetic energy of the element:

$$T^{(e)} = \frac{1}{2}\int_e \dot{\mathbf{r}}_{P\in e}^T \dot{\mathbf{r}}_{P\in e} dm = \frac{1}{2}\dot{\mathbf{q}}^{(e)^T}\left(\int_V \rho \mathbf{S}^T\mathbf{S} dV\right)\dot{\mathbf{q}}^{(e)} \tag{11}$$

The term between parentheses on the last term of equation (11) is the element mass matrix. It does not depend on the nodal coordinates nor on nodal velocities, which makes it specially suitable to be introduced on the equations of motion (1). If one splits the infinitesimal volume into the natural scaled coordinates of the element, the mass matrix of each element can be obtained by

$$\mathbf{M}^{(e)} = \int_{\xi^\star}\int_{\eta^\star}\int_{\zeta^\star} \rho \mathbf{S}^T\mathbf{S} d\zeta^\star d\eta^\star d\xi^\star \tag{12}$$

Assuming an isotropic linear elastic material, the elastic potential energy (Hughes, 2000; Lai et al., 2010) is

$$U^{(e)} = \frac{1}{2}\int_e \boldsymbol{\varepsilon} : \mathbf{D} : \boldsymbol{\varepsilon} dV \tag{13}$$

where ":" is a tensor contraction operation, $\boldsymbol{\varepsilon}$ is the Green-Lagrange strain tensor and $\mathbf{D}$ is the material constitutive tensor. By taking the partial derivative of the elastic energy with respect to each nodal degree of freedom, the elastic nodal force vector can be obtained:

$$\mathbf{f}^{(e)} = \frac{\partial U^{(e)}}{\partial \mathbf{q}^{(e)}} = \int_{\xi^\star}\int_{\eta^\star}\int_{\zeta^\star}\left(\frac{\partial \varepsilon}{\partial \mathbf{q}^{(e)}} : \mathbf{D} : \varepsilon\right)\det(\mathbf{J_0})d\zeta^\star d\eta^\star d\xi^\star \tag{14}$$

The term $\mathbf{J_0} = \partial \mathbf{r}_{0_{P\in e}}/\partial \boldsymbol{\xi}^\star$ is the Jacobian of the initial configuration and is an identity operator if the beam element is initially straight.

From the continuum mechanics theory, considering small strains, the Green-Lagrange strain tensor can be calculated from the deformation gradient $\mathbf{F} = \frac{\partial \mathbf{r}_{P\in e}}{\partial \boldsymbol{\xi}^\star}\mathbf{J}_0^{-1}$:

$$\boldsymbol{\varepsilon} = \frac{1}{2}\left(\mathbf{F}^T\mathbf{F} - \mathbf{I}\right) \tag{15}$$

To simplify what follows, the matrix $\mathbf{W} = \frac{d\mathbf{S}}{d\boldsymbol{\xi}}$ is defined as:

$$\mathbf{W} = \begin{bmatrix} S_{x,\xi} & S_{x,\eta} & S_{x,\zeta} \\ S_{y,\xi} & S_{y,\eta} & S_{y,\eta} \\ S_{z,\xi} & S_{z,\eta} & S_{z,\eta} \end{bmatrix}$$

Then, by using equation (6) and rearranging the terms, one can reach:

$$\frac{\partial \boldsymbol{\varepsilon}}{\partial \mathbf{q}^{(e)}} = \mathbf{J}_0^{-T}\mathbf{Q}^T\mathbf{W}^T\mathbf{W}\frac{\partial \mathbf{Q}}{\partial \mathbf{q}^{(e)}}\mathbf{J}_0^{-1} \tag{16}$$

where

$$\mathbf{Q} = \begin{bmatrix} \mathbf{q}^{(e)} & \mathbf{0} & \mathbf{0} \\ \mathbf{0} & \mathbf{q}^{(e)} & \mathbf{0} \\ \mathbf{0} & \mathbf{0} & \mathbf{q}^{(e)} \end{bmatrix}$$

and $S_{x,\xi}$ indicates the derivative of the first line of S, which is S_x, with respect to the natural coordinate ξ - and analogously for the other similar symbols.

It is useful to note here that equation (17) yields a third order tensor $\frac{\partial \boldsymbol{\varepsilon}}{\partial \mathbf{q}^{(e)}} = \left[\varepsilon'_{ijk,m}\right]$ that can be written in index notation as

$$\varepsilon'_{ij,m} = \frac{\partial \varepsilon_{i,j}}{\partial q_m^{(e)}} = \mathbf{J}_0^{-T}\mathbf{Q}^T\mathbf{W}^T\mathbf{W}\frac{\partial \mathbf{Q}}{\partial q_m^{(e)}}\mathbf{J}_0^{-1} \tag{17}$$

Now equation (17) can be feed into equation (18), which must be integrated to yield to elastic nodal force vector. As noted before, however, the integration of equation (18) stiffens the element and a reduced selective integration (Nachbagauer, 2014) technique can be used to avoid Poisson locking effect. This is carried out by splitting the material constitutive tensor into an extension $\mathbf{D}_0$ and a shear part $\mathbf{D}_\nu$ and modifying the equation for the elastic forces to the following form:

$$\mathbf{f}^{(e)} = \int_{\xi^\star}\int_{\eta^\star}\int_{\zeta^\star}\left(\frac{\partial \boldsymbol{\varepsilon}}{\partial \mathbf{q}^{(e)}} : \mathbf{D}_0 : \varepsilon\right)\det(\mathbf{J_0})d\zeta^\star d\eta^\star d\xi^\star + A^{(e)}\int_{\xi^\star}\left(\frac{\partial \boldsymbol{\varepsilon}}{\partial \mathbf{q}^{(e)}} : \mathbf{D}_\nu : \varepsilon\right)\det(\mathbf{J_0})d\xi^\star \tag{18}$$

where $A^{(e)}$ represents the cross-section area.

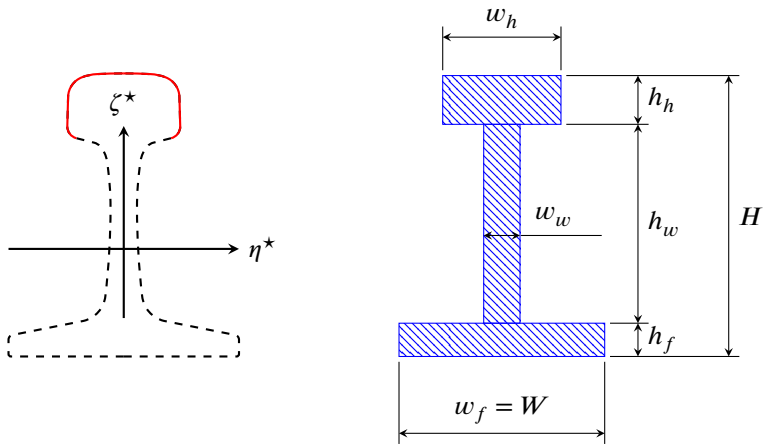

Figure 3 – Rail profile coordinate orientation (with TR68 profile) and simplified cross-section.

Now the multibody equations (1) can be extended to comprise also the flexible bodies, yielding:

$$\begin{bmatrix} \mathbf{M}_r & \mathbf{0} & -\mathbf{G}_r^T \\ \mathbf{0} & \mathbf{M}_f & -\mathbf{G}_f^T \\ \mathbf{G} & \mathbf{G}_f & \mathbf{0} \end{bmatrix} \begin{bmatrix} \ddot{\mathbf{z}} \\ \ddot{\mathbf{q}}_f \\ \lambda \end{bmatrix} = \begin{bmatrix} -\mathbf{h}_r \\ \mathbf{0} \\ \mathbf{0} \end{bmatrix} + \begin{bmatrix} \mathbf{f}_r \\ \mathbf{f}_f \\ \mathbf{0} \end{bmatrix} \tag{19}$$

where the subscripts r and f refer to rigid and flexible bodies respectively. The flexible mass matrix $\mathbf{M}_f$ must be assembled from the individual elemental mass matrices in equation (12) according to the nodal connectivity. Likewise, the elementary force vector in equation (18) is used to assemble $\mathbf{f}_f$.

A rail element

A rail used in railway transportation has standard profiles in which the width of the cross-section changes with height (figure 3). To perform an exact calculation of the rail beam element, then, equations (12) and (18) must be solved with integration limits $\eta^\star$ that depend on $\zeta^\star$. To simplify the integration process, the cross section can be divided into three rectangular cross sections representing the rail foot (the part connected to the sleepers), rail web, and rail head. Each one of these three sections have its respective height and width, and the resulting cross-section must have structural properties that matches the original rail profile.

With that simplification, the first term of Eq. (18) can be calculated separately for each of the three subareas. One can also drop the starred version of the natural coordinates and replace them by the non-scaled natural coordinates ξ, ζ, and η by performing a variable substitution:

$$\begin{aligned} \mathbf{f}^{(e)} = & \frac{Lh_f w_f}{8} \int_{-1}^{1}\int_{-1}^{1}\int_{-1}^{\zeta_f} \left(\frac{\partial \varepsilon}{\partial \mathbf{q}^{(e)}} : \mathbf{D}_0 : \varepsilon \right) \det(\mathbf{J_0}) d\zeta d\eta d\xi + \\ & + \frac{Lh_w w_w}{8} \int_{-1}^{1}\int_{-1}^{1}\int_{\zeta_f}^{\zeta_h} \left(\frac{\partial \varepsilon}{\partial \mathbf{q}^{(e)}} : \mathbf{D}_0 : \varepsilon \right) \det(\mathbf{J_0}) d\zeta d\eta d\xi + \\ & + \frac{Lh_h w_h}{8} \int_{-1}^{1}\int_{-1}^{1}\int_{\zeta_h}^{1} \left(\frac{\partial \varepsilon}{\partial \mathbf{q}^{(e)}} : \mathbf{D}_0 : \varepsilon \right) \det(\mathbf{J_0}) d\zeta d\eta d\xi + \\ & + A^{(e)} \frac{L}{2} \int_{-1}^{1} \left(\frac{\partial \varepsilon}{\partial \mathbf{q}^{(e)}} : \mathbf{D}_\nu : \varepsilon \right) \det(\mathbf{J_0}) d\xi \end{aligned} \tag{20}$$

where the integration limits are:

$$\zeta_f = -1 + 2\frac{h_f}{H}$$
$$\zeta_h = 1 - 2\frac{h_h}{H}$$

Likewise, Eq. 12 must be calculated for each subsection as:

$$\begin{aligned}\mathbf{M}^{(e)} = &\frac{Lw_f h_f}{8}\int_{-1}^{1}\int_{-1}^{1}\int_{-1}^{\zeta_f}\rho\mathbf{S}^T\mathbf{S}d\zeta d\eta d\xi + \\ &+\frac{Lw_w h_w}{8}\int_{-1}^{1}\int_{-1}^{1}\int_{\zeta_f}^{\zeta_h}\rho\mathbf{S}^T\mathbf{S}d\zeta d\eta d\xi + \\ &+\frac{Lw_h h_h}{8}\int_{-1}^{1}\int_{-1}^{1}\int_{\zeta_h}^{1}\rho\mathbf{S}^T\mathbf{S}d\zeta d\eta d\xi\end{aligned} \tag{21}$$

Shape functions

The shape functions used for this paper results were the same applied by Nachbagauer et al. (2011):

$$\mathbf{S} = \begin{bmatrix}\mathbf{S}_1 & \mathbf{S}_2 & \mathbf{S}_3 & \mathbf{S}_4 & \mathbf{S}_5 & \mathbf{S}_6 & \mathbf{S}_7 & \mathbf{S}_8 & \mathbf{S}_9\end{bmatrix} = \begin{bmatrix}S_x \\ S_y \\ S_z\end{bmatrix} \tag{22}$$

where

$$\mathbf{S}_i = \begin{bmatrix}S_i & 0 & 0 \\ 0 & S_i & 0 \\ 0 & 0 & S_i\end{bmatrix} \tag{23}$$

such that

$$\begin{aligned}S_1 &= -\frac{\xi}{2}(1-\xi) & S_2 &= \eta S_1 & S_3 &= \zeta S_1 \\ S_4 &= 1-\xi^2 & S_5 &= \eta S_4 & S_6 &= \zeta S_4 \\ S_7 &= \frac{\xi}{2}(1+\xi) & S_8 &= \eta S_7 & S_9 &= \zeta S_7\end{aligned}$$

Linearization

Displacements on rails are usually small compared to its length. For most situations, then, it is reasonable to use a linearized version of the nodal force vector from Eq. (18). A Taylor series expansion around a reference configuration where the nodal coordinates are $\mathbf{q}_s^{(e)}$ would read:

$$\mathbf{f}^{(e)} = \mathbf{f}_s^{(e)} + \frac{d\mathbf{f}^{(e)}}{d\mathbf{q}^{(e)}}\left(\mathbf{q}^{(e)} - \mathbf{q}_s^{(e)}\right) + \mathcal{O}_2 \approx \mathbf{f}_s^{(e)} + \mathbf{K}_r^{(e)}\left(\mathbf{q}^{(e)} - \mathbf{q}_s^{(e)}\right) \tag{24}$$

where $\mathbf{f}_r^{(e)=\mathbf{f}^{(e)}(\mathbf{q}_r)}$ and $\mathbf{K}_r^{(e)}$ is the element tangent stiffness matrix. With that simplification, one can retain the convenient constant representation of the ANCF mass matrix for large rotations and translations, while avoiding the cumbersome calculation of the complete non-linear force vector.

RESULTS

In the following, some results from simulations carried out with the proposed element are shown. The first set of simulations comprise of static calculations of a beam fixed at one end, and subjected to a vertical load on the opposing end.

Table 1 – Simplified cross-section area properties and errors compared to nominal TR68 properties.

Property	Simplified section	Error / %
Area	8700 mm	0.012
Moment $I_{\eta^\star}$	39×10^6 mm^4	0.35
Moment $I_{\zeta^\star}$	6.0×10^6 mm^4	−0.023
Centroid height	85 mm	−0.00000047

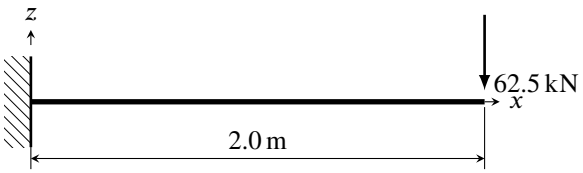

Figure 4 – Static test problem.

Beam under simple static bending

The AREMA TR68 rail have a cross-sectional area of 8700 mm^2, second area moment around centroidal axis $\eta^\star$ of 39×10^6 mm^4, second area moment of inertia around centroidal axis $\zeta^\star$ of 6.0×10^6 mm^4, and centroid height of 85 mm. By fixing the total section height to be the same as the standard profile (190 mm) and performing an error minimization procedure using Newton's method, the following set of dimensions were found: $w_b = 140$ mm, $h_b = 22$ mm, $w_w = 24$ mm, $h_w = 130$ mm, $w_h = 78$ mm, and $h_h = 32$ mm. Table 1 shows the properties of the simplified cross-section session compared to the original, standard TR68 profile.

To verify the element performance, a static test was setup using a 2.0 m long rail, fixed at its left edge and with a vertical load of 63 kN applied to the other edge, as shown in Fig. 4. The rail is considered to be initialy horizontal. Four simulations were carried out using different element configurations:

- a non-linear ANCF element with rectangular cross-section with $I_{\eta^\star}$ that match the ones from the AREMA TR68 rail;
- a non-linear ANCF rail element with the simplified cross-section approach described in this paper and properties as presented in Tab. 1;
- a linearized ANCF rail element with the same cross-section characteristics as above;
- a B23 Abaqus beam element with general cross-section and properties from the AREMA TR68 rail profile.

For all cases, the 2.0 m beam was discretized using 10 elements of 0.20 m. In the case of the elements proposed in this paper, the implementation was carried out in Python and the routine `fsolve` from the Scipy package was used to find the equilibrium configuration of the rail. Figure 5 presents the final configuration of the neutral fiber of the rail for the simulated cases. It can be seen that results were very close.

Table 2 shows the displacements of the tip of the beam subjected to the vertical load. One can verify that the proposed rail element vertical (z) displacements are in good agreement with the Abaqus B32 element, and with the equivalent rectangular element as well.

Table 2 – Free edge displacements of the test beam

Case	z displacement / m	x displacement / m
ACNF rectangular element	-2.06737×10^{-2}	-1.27676×10^{-4}
Proposed rail element	-2.11837×10^{-2}	8.36648×10^{-4}
Proposed rail element (linearized)	-2.11668×10^{-2}	9.70630×10^{-4}
Abaqus B32 element	-2.14434×10^{-2}	-1.40000×10^{-4}

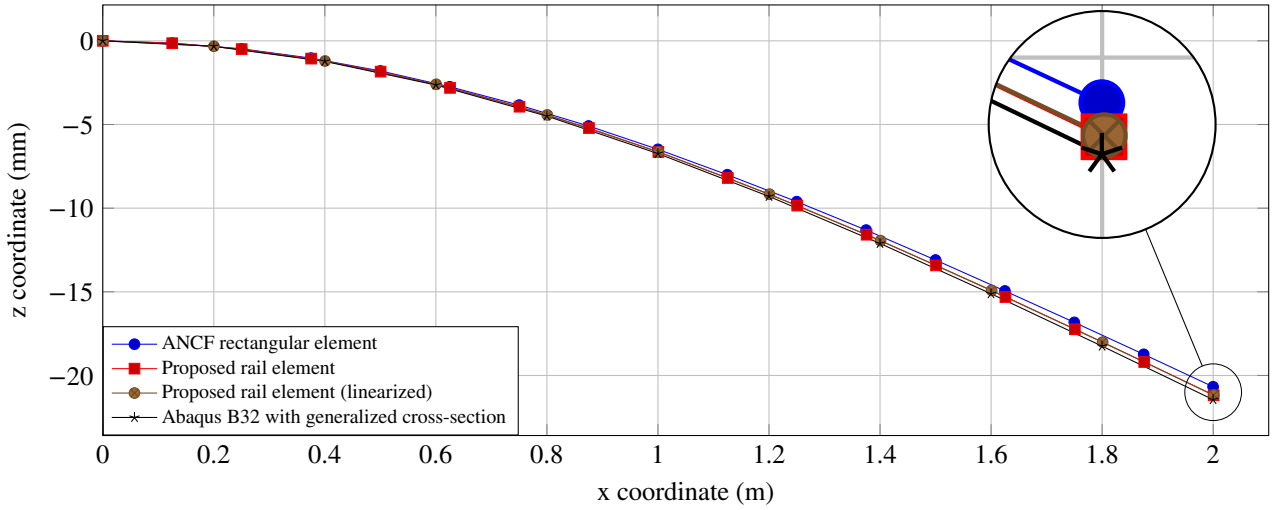

Figure 5 – Comparison between final shape of the neutral line for: (a) a rectangular ANCF element with cross-section properties equivalent to TR68; (b) the proposed rail ANCF element with non-linearized force calculation, and (c) linearized force calculation; (d) Abaqus B32 elements with generic cross section with TR68 properties.

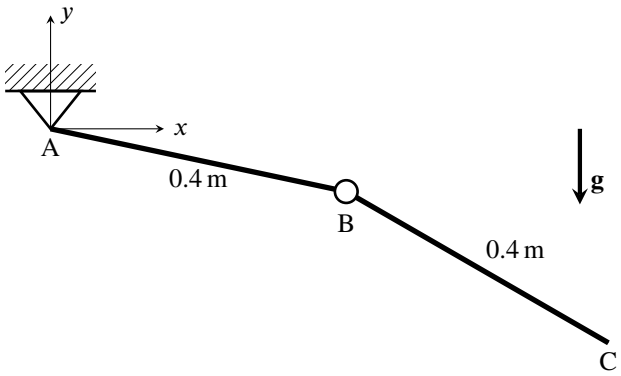

Figure 6 – Double pendulum example

Double pendulum

The previous results confirmed that the proposed element can achieve similar static results as other types of elements and implementations. To verify its behavior under dynamic circumstances, a double pendulum example was set up, as shown in Figure 6. The system is composed of two three-dimensional, 0.40 m long beams with rectangular cross-section with height of 20 mm and width of 30 mm. Both are made of an elastic material with Young's modulus of 210 MPa, Poisson's coefficient 0.30, and density 7900 $\mathrm{kg\,m^{-3}}$.

The proposed element was solved using a simple Euler time-stepping scheme, and then also with the IDA solver from the SUNDIALS package (implemented via the Asimulo Python library). Comparative results are presented against the same system modeled using Abaqus/Standard's B23 elements, and Simpack's linear SIMBEAMS elements. The linear SIMBEAM approach presented uses a modal reduction in order to save simulation times.

Results, shown in Figure 7, are very similar to the four cases, but start to diverge when the first oscillation of the beam that is pinned to the ground ends. When that happens, it can be seen the the proposed element results are in good agreement with the Abaqus model, and more so when the more robust IDA solver is used. The SIMBEAM element, however drifts away from the positions predicted by Abaqus and by the proposed element.

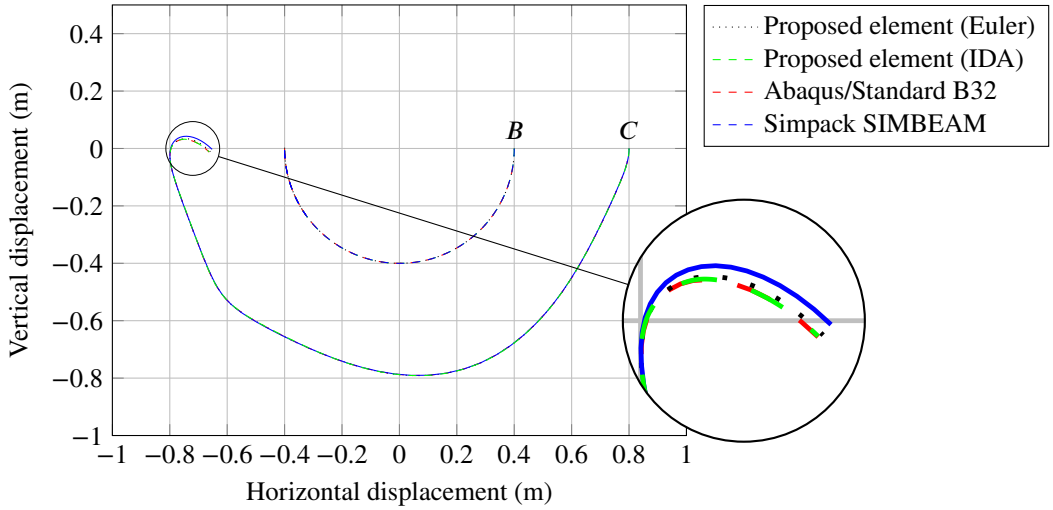

Figure 7 – Results for the dynamic simulation of a double pendulum. Curves show the trajectory of points B and C from Figure 6

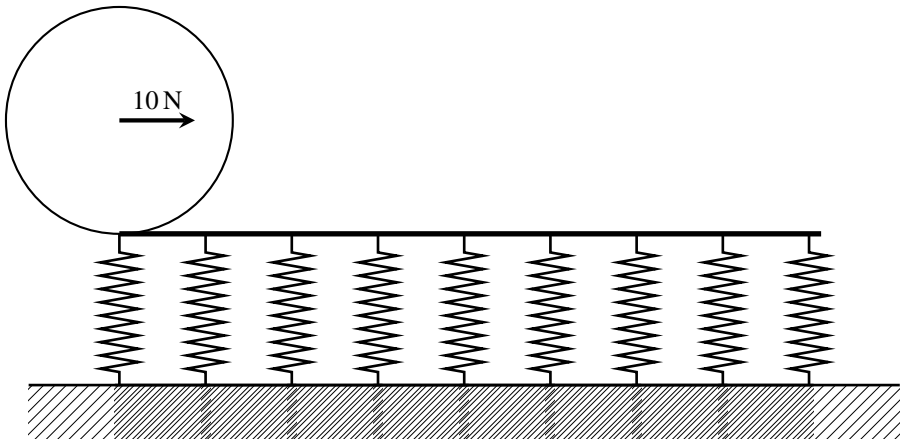

Figure 8 – Wheelset on flexible rail. Vertical section.

Wheelset on rails with sleepers

Finally, an example with a railway vehicle wheelset supported by rails over sleepers was developed, Figure 8. General mechanical properties are shown in Table 3. The wheels are considered to be cylindrical, and the rails use AREMA TR68 profiles, with track width of 1.0 m. No friction between wheel and rails is considered.

At first, the wheelset is released from its initial position and let rest for 1 second, in order to accommodate on the rails. Then, a 10 N horizontal force is input on its center of mass.

CONCLUSIONS

In this paper, a method to consider a rail profile is proposed to enhance quadratic beam elements written in the absolute nodal coordinate formulation. Preliminary results suggest that the element can adequately model rails used in railroads inside a multibody framework.

Table 3 – Properties of the wheelset on rails simulation.

Property	**Value**
Wheelset mass	$100\,\mathrm{kg}$
Wheelset polar inertia	$1.1\,\mathrm{kg\,m^2}$
Wheelset transverse inertias	$8.3\,\mathrm{kg\,m^2}$
Number of elements per rail	4
Element length	$1.6\,\mathrm{m}$
Vertical sleeper stiffness	$3.0\times10^{6}\,\mathrm{N\,m^{-1}}$
Vertical sleeper damping	$3.0\times10^{4}\,\mathrm{N\,s\,m^{-1}}$
Lateral sleeper stiffness	$1.4\times10^{9}\,\mathrm{N\,m^{-1}}$
Lateral sleeper damping	$29\times10^{6}\,\mathrm{N\,s\,m^{-1}}$

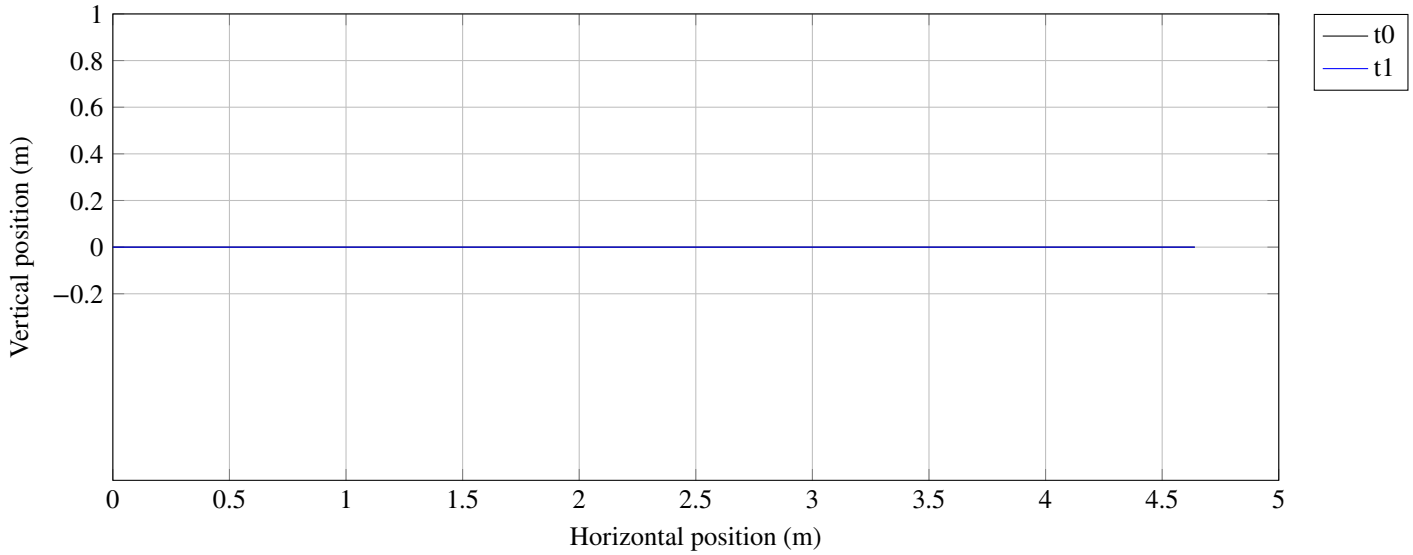

Figure 9 – Caption

REFERENCES

Antunes, P., Magalhães, H., Ambrósio, J., Pombo, J., and Costa, J. (2019). A co-simulation approach to the wheel–rail contact with flexible railway track. *Multibody System Dynamics*, 45(2):245–272.

Ascher, U. M. and Petzold, L. R. (1998). *Computer methods for ordinary differential equations and differential-algebraic equations*. Society for Industrial and Applied Mathematics, Philadelphia.

Berzeri, M., Campanelli, M., and Shabana, A. A. (2001). Definition of the Elastic Forces in the Finite-Element Absolute Nodal Coordinate Formulation and the Floating Frame of Reference Formulation. *Multibody System Dynamics*, 5:21–54.

Berzeri, M. and Shabana, A. A. (2000). Development of simple models for the elastic forces in the absolute nodal co-ordinate formulation. *Journal of Sound and Vibration*, 235(4):539–565.

Escalona, J. L., Hussien, H. A., and Shabana, A. A. (1998). Application of the absolute nodal co-ordinate formulation to multibody system dymamics. *Journal of Sound and Vibration*, 214(5):833–851.

Evans, J. and Berg, M. (2009). Challenges in Simulation of Rail Vehicle Dynamics. *Vehicle System Dynamics*, 47(8):1023–1048.

Guimarães, C. A. B. (1999). *Análise das Solicitações Dinâmicas na Via Férrea através da Simulação da Interação entre o Veículo e a Via*. PhD Thesis, Faculdade de Engenharia Mecânica, Campinas.

Hughes, T. J. R. (2000). *The Finite Element Method: Linear Static and Dynamic Finite Element Analysis (Dover Civil and Mechanical Engineering)*. Dover Publications.

Knothe, K. and Grassie, S. (1993). Modelling of Railway Track and Vehicle/Track Interaction at High Frequencies. *Vehicle System Dynamics*, 22(3-4):209–262.

Lai, W. M., Rubin, D., and Krempl, E. (2010). *Introduction to continuum mechanics*. Butterworth-Heinemann/Elsevier, Amsterdam ; Boston, 4th ed edition. OCLC: ocn300722280.

Lima, E. A., Baruffaldi, L. B., Manetti, J. L. d. B., Santos, Jr, A. A. d., and Martins, T. (2022). Effect of truck shear pads on the dynamic behaviour of heavy haul railway cars. *Vehicle System Dynamics*, 60(4).

Nachbagauer, K. (2014). State of the Art of ANCF Elements Regarding Geometric Description, Interpolation Strategies, Definition of Elastic Forces, Validation and the Locking Phenomenon in Comparison with Proposed Beam Finite Elements. *Archives of Computational Methods in Engineering*, 21(3):293–319.

Nachbagauer, K., Gruber, P., and Gerstmayr, J. (2013a). A 3D Shear Deformable Finite Element Based on the Absolute Nodal Coordinate Formulation. In Samin, J.-C. and Fisette, P., editors, *Multibody Dynamics*, volume 28, pages 77–96. Springer Netherlands, Dordrecht. Series Title: Computational Methods in Applied Sciences.

Nachbagauer, K., Gruber, P., and Gerstmayr, J. (2013b). Structural and Continuum Mechanics Approaches for a 3D Shear Deformable ANCF Beam Finite Element: Application to Static and Linearized Dynamic Examples. *Journal of Computational and Nonlinear Dynamics*, 8(2):021004.

Nachbagauer, K., Pechstein, A., Irschik, H., and Gerstmayr, J. (2011). A new locking-free formulation for planar, shear deformable, linear and quadratic beam finite elements based on the absolute nodal coordinate formulation. *Multibody System Dynamics*, 26(3):245–263.

Pfeiffer, F. (2005). *Mechanical Systems Dynamics*. Springer, Berlim.

Recuero, A. M., Escalona, J. L., and Shabana, A. A. (2011). Finite-element analysis of unsupported sleepers using three-dimensional wheel–rail contact formulation. *Proceedings of the Institution of Mechanical Engineers, Part K: Journal of Multi-body Dynamics*, 225(2):153–165.

Shabana, A. (2005). *Dynamics of multibody systems*. Cambridge University Press, Cambridge, 3 edition. https://doi.org/10.1017/CBO9780511610523.

Shabana, A. A., Chamorro, R., and Rathod, C. (2008). A multi-body system approach for finite-element modelling of rail flexibility in railroad vehicle applications. *Proceedings of the Institution of Mechanical Engineers, Part K: Journal of Multi-body Dynamics*, 222(1):1–15.

Shabana, A. A. and Christensen, A. P. (1997). Three-dimensional absolute nodal co-ordinate formulation: plate problem. *International Journal for Numerical Methods in Engineering*, 40(15):2775–2790.

Shabana, A. A., Hussien, H. A., and Escalona, J. L. (1997). Absolute Nodal Coordinate Formulation. In *Volume 1A: 16th Biennial Conference on Mechanical Vibration and Noise*, page V01AT06A016, Sacramento, California, USA. American Society of Mechanical Engineers.

Shabana, A. A. and Sanborn, G. (2009). An alternative simple multibody system approach for modelling rail flexibility in railroad vehicle dynamics. *Proceedings of the Institution of Mechanical Engineers, Part K: Journal of Multi-body Dynamics*, 223(2):107–120.

Shabana, A. A. and Yakoub, R. Y. (2001a). Three Dimensional Absolute Nodal Coordinate Formulation for Beam Elements: Implementation and Applications. *Journal of Mechanical Design*, 123(4):614–621.

Shabana, A. A. and Yakoub, R. Y. (2001b). Three Dimensional Absolute Nodal Coordinate Formulation for Beam Elements: Theory. *Journal of Mechanical Design*, 123(4):606–613.

Timoshenko, S. P. (1926). Method of Analysis of Statical and Dynamical Stresses in Rail. In *Proc. of 2nd. International Congress for Applied Mechanics*, pages 407–418, Zurique.

Winkler, E. (1867). *Die Lehre von der Elasticitaet und Festigkeit: mit besonderer Rücksicht auf ihre Anwendung in der Technik*.

RESPONSIBILITY NOTICE

The authors are the only parties responsible for the printed material included in this paper.